




Article

Self-Heating Ability of Geopolymers Enhanced by Carbon Black Admixtures at Different Voltage Loads

Lukáš Fiala ^{1,*}, Michaela Petříková ¹, Wei-Ting Lin ², Luboš Podolka ³ and Robert Černý ¹

¹ Department of Materials Engineering and Chemistry, Faculty of Civil Engineering, Czech Technical University in Prague, Thákurova 7, 166 29 Prague 6, Czech Republic; michaela.petrkova@fsv.cvut.cz (M.P.); cernyr@fsv.cvut.cz (R.C.)

² Department of Civil Engineering, College of Engineering, National Ilan University, No.1, Sec. 1, Shennong Rd., I-Lan 260, Taiwan; wtlin@niu.edu.tw

³ Department of Civil Engineering, Faculty of Technology, Institute of Technology and Business in České Budějovice, Okružní 517/10, 370 01 České Budějovice, Czech Republic; podolka@mail.vstecb.cz

* Correspondence: fialal@fsv.cvut.cz; Tel.: +420-22435-7125

Received: 20 September 2019; Accepted: 25 October 2019; Published: 29 October 2019



Abstract: Sustainable development in the construction industry can be achieved by the design of multifunctional materials with good mechanical properties, durability, and reasonable environmental impacts. New functional properties, such as self-sensing, self-heating, or energy harvesting, are crucially dependent on electrical properties, which are very poor for common building materials. Therefore, various electrically conductive admixtures are used to enhance their electrical properties. Geopolymers based on waste or byproduct precursors are promising materials that can gain new functional properties by adding a reasonable amount of electrically conductive admixtures. The main aim of this paper lies in the design of multifunctional geopolymers with self-heating abilities. Designed geopolymer mortars based on blast-furnace slag activated by water glass and 6 dosages of carbon black (CB) admixture up to 2.25 wt. % were studied in terms of basic physical, mechanical, thermal, and electrical properties (DC). The self-heating ability of the designed mortars was experimentally determined at 40 and 100 V loads. The percolation threshold for self-heating was observed at 1.5 wt. % of carbon black with an increasing self-heating performance for higher CB dosages. The highest power of 26 W and the highest temperature increase of about 110 °C were observed for geopolymers with 2.25 wt. % of carbon black admixture at 100 V.

Keywords: geopolymers; ground-granulated blast-furnace slag; carbon black; self-heating

1. Introduction

Building materials with new functional properties that extend their usability in sophisticated applications, so-called multifunctional or smart materials, are currently in high demand by the construction industry. Studies dealing with their design, experimental determination of material properties, and testing of newly achieved abilities have been, and still are, mainly focused on cementitious composites. A comprehensive review dealing with a definition and classification of smart concretes and structures and possible applications introduced by Han et al. [1] showed that a variety of possible enhancements exist. Some of the new functional properties, such as self-sensing, self-heating, energy harvesting, or electromagnetic shielding/absorbing, are crucially dependent on electrical properties that are, in the case of common aluminosilicate-based building materials, often very poor. Therefore, some electrically conductive admixtures are necessary for the formation of a conductive net within the material matrix. Much effort has been devoted to studies dealing with influence of carbon-based and metallic admixtures on new functional properties of cementitious

materials. For example, Rana et al. [2] introduced a review focused on utilization of carbon-based materials such as carbon fibers (CFs), carbon nanofibers (CNFs), and carbon nanotubes (CNTs) in self-sensing cementitious materials; Han et al. [3] reviewed the self-sensing properties of cementitious materials with nanocarbon admixtures, namely CNFs, CNTs, and nano graphite platelets (NGPs); the review of Li et al. [4] was focused on research performed on cementitious composites with nano titanium dioxide (NT) and concluded that such materials possess self-sensing properties; and Pisello et al. [5] performed a detailed characterization of cementitious materials with multiwalled carbon nanotubes (MWCNTs), CNFs, carbon black (CB), and graphene nanoplatelets (GNPs) and, based on results, concluded that MWCNTs optimized piezoresistive properties and the tested nanofillers could be useful for cementitious smart materials and energy efficiency optimization.

The self-heating ability of cement-matrix and polymer-matrix composites with steel fibers (SFs) and CFs for deicing and space heating was reviewed by Chung [6]. Gomis et al. [7] studied in experimental and theoretical ways the self-heating ability of cement pastes with graphite powder (GP), carbon fiber powder (CFP), CFs, CNFs, and CNTs and, according to experiments conducted on samples with dimensions $100 \times 100 \times 10 \text{ mm}^3$ loaded by 50, 100, and 150 V DC, concluded that the self-heating ability of such materials is convenient in preventing the formation of ice layers in transportation infrastructures. Armoosh and Oltulu [8,9] investigated the self-heating ability of cementitious composites with metallic admixtures, iron, copper, and brass shavings, up to 20%, and proved the self-heating ability under a voltage load in the range of 20–60 V.

Wei et al. presented within several works the energy harvesting ability of cementitious materials with different electrically conductive admixtures, namely expanded graphite (EG) [10], CNT [11], and CF [12]. Despite the fact that the energy-harvesting efficiency of such materials is not high, it is promising large surface area of constructions usable for harvesting securing reasonable energy profit.

In general, cementitious materials are currently the most frequently used construction materials worldwide. Global production of cement has grown rapidly in recent years [13,14], and it is the third-largest source of anthropogenic emissions of carbon dioxide, after fossil fuels, deforestation, and other land-use changes. Global cement production has increased more than 30 times since 1950, and global process emissions in 2017 were $1.48 \pm 0.20 \text{ Gt CO}_2$. Cumulative emissions from 1928 to 2017 were $36.9 \pm 2.3 \text{ Gt CO}_2$, of which 70% has occurred since 1990 [15]. Taking into account the high negative impact of cement production on the environment, the design of building materials with comparable material properties to cementitious materials, but with a lower environmental impact of their production, is justified.

Geopolymers are inorganic materials of an environmentally friendly nature thanks to their fundamental component, so-called precursor, that is usually waste or byproduct originating from various types of industrial production [16]. A comprehensive review of precursors and alkali activators was introduced by Ma et al. [17], with a conclusion that geopolymers present better mechanical properties, a higher durability, and a more desirable structural performance compared to their conventional counterparts. Based on experiments, Albitar et al. [18] concluded that geopolymers are more chemically stable, superior to conventional concrete in an acidic environment, and exhibit lower deterioration of mechanical properties under chemical attacks. Good resistance at high temperatures was experimentally proved by Zuda et al. [19]. Taking into account the good material properties and lower impact on the environment than of cementitious materials, geopolymers can find an application in building practices.

Geopolymer binders are formed by the reaction of alkalis with amorphous aluminosilicate-rich precursors whose composition determines the material structure that is formed during hydration. In high-calcium systems (blast-furnace slag), typically calcium alumina-silicate hydrated gel (C-A-S-H) is formed [20], whereas in low-calcium systems (fly-ash, metakaolin, clay), sodium alumina-silicate hydrated gel (N-A-S-H) is present [21]. Alkali activation can be carried out by various alkali-activators, such as alkali hydroxides, weak or strong acid salts, silicates, aluminates, or aluminosilicates [22]. In general, the higher the alkalinity of the activator, the faster the initial reaction of the activator with

precursor. The differences in heat evolution of slag activated by NaOH, water glass, and a combination of NaOH and water glass were presented by Altan and Erdogan [23], and a faster initial reaction was observed in NaOH by isothermal calorimetric measurements by Haha et al. [24]. Mostly used alkaline activators are mixtures of sodium or potassium hydroxide (NaOH, KOH) with sodium or potassium water glass ($n\cdot\text{SiO}_2\cdot\text{Na}_2\text{O}$, $n\cdot\text{SiO}_2\cdot\text{K}_2\text{O}$) [25].

Multifunctional geopolymers can be designed in a similar way to multifunctional cementitious materials by the addition of electrically conductive admixtures [26]. However, the design of multifunctional geopolymers and their acquired abilities are not so well explored. Rovnaník et al. [27] compared self-sensing properties of alkali-activated slag mortars with Portland cement mortars and concluded that, due to some content of iron particles in slag, an applicable sensitivity is evident in practice, even without any electrically conductive admixture, whereas in the case of Portland cement, mortar self-sensing is detectable but not sufficient for practical applications. Another similar study performed by Rovnaník et al. [28] dealt with the self-sensing ability of a geopolymer mortar based on slag activated by water glass with GP admixture. They concluded that such materials exhibit a self-sensing ability but with a significant decrease in compressive strength. Concerning the self-heating ability, it was experimentally confirmed on small alkali-activated slag samples with a CB admixture in the amount of 8.89 wt. % at 32.1 and 41.5 V by Fiala et al. [29]

Slag as a high-calcium precursor is a solid waste generated by the iron and steel industry. In 2014, slag was produced in the amount of 250 Mt within the 1.6 Gt of global steel production [30]. In 2013, the annual slag production of one of the leading producers, China, reached more than 100 million tons with just 29.5% utilization rate, which is very low in comparison to industrial countries. The utilization rate reaches 98.4% in Japan, 87.0% in Europe, and 84.4% in the United States. As of 2016, more than 300 million tons of accumulated steel slag has not been used effectively in China, which, taking into account large steel slag emissions, causes an important environmental problem for China [31]. Slag in granulated form is a precursor that can be relatively easily alkali-activated, and originating geopolymers can be used in the construction industry.

Within the research presented in this paper, granulated blast-furnace slag (GBFS) was used as a precursor for alkali activation by water glass, and CB admixtures were added in various dosages in order to enhance the effective electrical properties of the designed geopolymers that would be promising in terms of the self-heating ability. Subsequently, material properties involving basic physical, mechanical, thermal, and electrical properties were experimentally determined, and self-heating tests were conducted in order to verify the self-heating ability of such materials. It was observed that the self-heating ability of the tested materials started from a CB amount of 1.5 wt. %, and such material is able to generate heat at a DC voltage of 40 V leading to a small temperature increase. The best self-heating performance was observed for geopolymers with 2.25 wt. % of CB at 100 V, where the temperature increase was about 110 °C in approximately one hour.

2. Materials and Methods

A high-calcium precursor, GBFS SMŠ 380 (39.8% CaO), produced by Kotouč Štramberk Ltd. was activated by water glass Susil produced by Vodní sklo a.s. GBFS is an industrial byproduct of iron production with a fineness of $380\text{ m}^2\cdot\text{kg}^{-1}$ (Blaine). The average grain size of the slag particles determined by laser granulometry was $d_{50} = 15.5\ \mu\text{m}$ and $d_{90} = 38.3\ \mu\text{m}$. Activation was performed by sodium silicate solution (water glass Susil MP 2.0 with a molar ratio $\text{SiO}_2/\text{Na}_2\text{O} = 2.07$). Three normalized CEN fractions of fine quartz sand (PG1, PG2, PG3) produced by Filtrační písky, Ltd., that complied with the ČSN EN 196-1 standard were used as a filler. The effective electrical properties of the composites were enhanced by CB VULCAN 7H. CB is essentially elemental carbon in the form of spherical particles and aggregated clusters of those particles with a high surface area and high electrical conductivity. The average grain size of CB particles was $d_{50} = 0.52\ \mu\text{m}$ and $d_{90} = 17.6\ \mu\text{m}$. In Figure 1, the particle size distribution of CB VULCAN 7H determined by laser granulometry is presented.

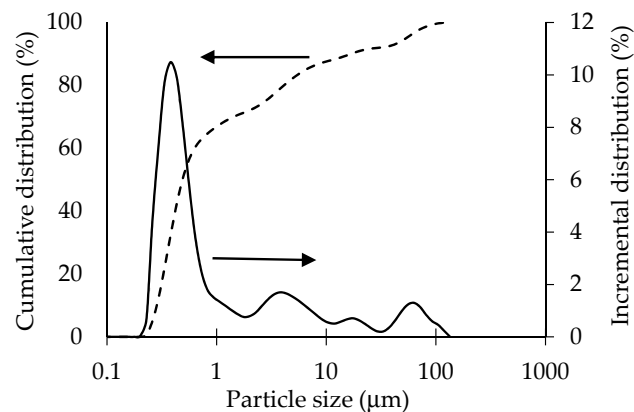


Figure 1. Particle size distribution of CB VULCAN 7H determined by laser granulometry.

CB VULCAN 7H is mainly manufactured for tires and industrial rubber production [32]. Its production is performed by thermal cracking of heavy aromatic feedstock, such as oil, in a hot flame. Oil is injected into a furnace hot flame zone where hydrocarbons are cracked to carbon and hydrogen by means of quenching the flame by water. Because of the reasonably high electrical conductivity and high surface area of such a way of processing CB, it can be used to optimize the electrical properties of polymers [33] and inorganic building materials [34,35].

In Table 1, the compositions of geopolymers with an optimized amount of mixing water are given. Seven different mixtures, the reference geopolymer (CB 0), and geopolymers with CB in the amounts of 0.75 wt. %, 1.25 wt. %, 1.5 wt. %, 1.75 wt. %, 2 wt. %, and 2.25 wt. % were designed and prepared by the following procedure. First, suspensions (10% and 15%) were prepared by adding a given amount of CB powder into water with nonionic surfactant Triton X-100 (Sigma-Aldrich, St. Louis, MO, USA) in the form of 0.5% solution and stirred by homogenizer IKA ULTRA-TURRAX for 15 min. An initial amount of additional water was then added to the GBFS suspension and stirred by a mixer for several minutes. In order to eliminate foaming during mixing leading to the formation of large pores, 1% solution of siloxane-based air-detraining agent Lukosan S (Lučební závody, Kolín, Czech Republic) was added. Subsequently, three fractions of sand were added to the mixture and stirred again by a mixer for several minutes. Consistency of fresh mixtures was tested according to the ČSN EN 1015-3 standard Determination of Consistence of Fresh Mortar by Flow Table, which is mainly used for cementitious mortars but is used also for alkali-activated ones [36]. The water-to-slag ratio of the mixtures was adjusted so that the average base diameter was equal to 160 mm, which is within the plastic range (140–200 mm) closer to the dry consistency bounds. Final mixtures with optimized water-to-slag ratios were then poured into molds and covered by a plastic cover. After one day, solidified samples were demolded and placed into a water bath for 28 d. Before the experiments (except the experimental determination of mechanical properties), samples were dried in an oven and subsequently cooled down in desiccator with silica gel.

Table 1. Compositions of the studied geopolymers.

	Carbon Black (CB) 0	CB 0.75	CB 1.25	CB 1.5	CB 1.75	CB 2	CB 2.25
Granulated blast-furnace slag (GBFS) (g)	100	100	100	100	100	100	100
Water glass (g)	20	20	20	20	20	20	20
Sand PG1 (g)	100	100	100	100	100	100	100
Sand PG2 (g)	100	100	100	100	100	100	100
Sand PG3 (g)	100	100	100	100	100	100	100
CB suspension (%)	0	10	10	10	15	15	15
CB amount (g)	0	3	5	6	7	8	9
Water-to-slag ratio (–)	0.44	0.60	0.69	0.74	0.77	0.81	0.84

The bulk density was determined on dry samples with dimensions of $50 \times 50 \times 50 \text{ mm}^3$ by means of the gravimetric method. The matrix density was determined on samples with dimensions of $50 \times 50 \times 50 \text{ mm}^3$ by means of the vacuum saturation method. With respect to the bulk density and the matrix density, the total open porosity Ψ (%) was calculated by the following equation

$$\Psi = 100 \cdot \left(1 - \frac{\rho_v}{\rho_{mat}} \right), \quad (1)$$

where ρ_v ($\text{kg}\cdot\text{m}^{-3}$) is the bulk density, and ρ_{mat} ($\text{kg}\cdot\text{m}^{-3}$) is the matrix density.

Mechanical properties were determined on three samples with dimensions of $40 \times 40 \times 160 \text{ mm}^3$ according to the Czech Standard ČSN EN 196-1. Samples cured for 28 d were first tested in terms of flexural strength by a three-point bending test. The length between the supports was 100 mm, and the loading rate was 0.15 mm/min. The compressive strength was then determined on six halves of the prisms originating from the previous flexural strength tests.

Thermal properties were determined on samples with dimensions $70 \times 70 \times 70 \text{ mm}^3$ by a commercial device ISOMET 2114 (Applied Precision, Ltd.) attached by a surface probe by means of the transient heat-pulse method. Such measurements were based on an analysis of the temperature response to the generated heat flow pulses. Heat flow was induced by electric heating using a resistor heater placed in the probe having direct thermal contact with the surface of the sample. First, the probe was heated up, and, subsequently, temperature decrease was monitored after the heater was turned off. With the known geometry of the probe and a decrease of the temperature due to dissipation of the heat in the sample, thermal properties were identified.

Electrical properties were measured in a two-probe arrangement in DC regime. First, the samples with dimensions $50 \times 50 \times 50 \text{ mm}^3$ were attached to electrodes where two opposite lateral sides were painted with a conductive carbon paint. Then, copper tape was pasted onto the first conductive layer in order to gain good contact of the samples with a power supply and wattmeter (self-heating experiment) and multimeter (electrical properties).

Resistance R (Ω) of the dried samples was measured by a Fluke 8846A $6\frac{1}{2}$ digit precise multimeter, and the electrical conductivity σ ($\text{S}\cdot\text{m}^{-1}$) was calculated with respect to the shape ratio of the samples (electrodes: $50 \times 50 \text{ mm}^2$, distance between electrodes: 50 mm) by the following equation

$$\sigma = \frac{1}{R} \cdot \frac{l}{S}, \quad (2)$$

where R (Ω) is the resistance of the sample, l (m) is the distance between electrodes, and S (m^2) is the area of electrodes.

Self-heating experiments were performed on samples with dimensions of $50 \times 50 \times 50 \text{ mm}^3$. Dried samples with electrodes attached in the same way as for determining the electrical properties were connected to a GW Instek GPR-11H30D voltage power supply and loaded by one or two voltage levels (Figure 2). Mortar samples CB 0 and CB 0.75 were loaded by 40 V to prove the no self-heating ability that was expected because of the electrical conductivity measurements. CB 1.25 mortar and mortars with higher amounts of CB were tested at two voltage levels, 40 and 100 V. Electrical power was monitored by a GW Instek GPM-8213 wattmeter. Ambient laboratory temperature and temperatures of samples were monitored by Pt-100 probes supported by Ahlborn ALMEMO 8690-9A datalogger in the central position of the bottom sides of the samples perpendicular to the attached electrodes.



Figure 2. (a) Samples for self-heating experiments. (b) Apparatus for self-heating experiments.

3. Results

3.1. Basic Physical Properties

In Table 2, the basic physical properties were represented by the bulk density, the matrix density, and the total open porosity. The bulk density was highest for the reference mortar CB 0 ($2111 \text{ kg}\cdot\text{m}^{-3}$) and decreased systematically with increasing CB amounts down to $1720 \text{ kg}\cdot\text{m}^{-3}$ (CB 2.25). The matrix density was in the range of $2562\text{--}2602 \text{ kg}\cdot\text{m}^{-3}$ and did not exhibit a significant influence on the amount of CB admixture. The total open porosity was calculated from the bulk density and the matrix density by Equation (1). It was lowest for CB 0 (17.6%) and exhibited an increasing tendency with increasing amounts of CB up to 33.4% (CB 2.25). Compared to the reference mortar, the addition of 0.75 wt. % of CB resulted in an increase in porosity of 7.6%, whereas addition of 2.25% wt. % of CB almost doubled the porosity (increase of 15.8%).

Table 2. Basic physical properties of the studied geopolymers.

	Bulk Density ($\text{kg}\cdot\text{m}^{-3}$)	Matrix Density ($\text{kg}\cdot\text{m}^{-3}$)	Total Open Porosity (%)
CB 0	2111	2562	17.6
CB 0.75	1947	2602	25.2
CB 1.25	1914	2588	26.0
CB 1.5	1816	2577	29.5
CB 1.75	1773	2568	31.0
CB 2	1749	2570	31.9
CB 2.25	1720	2582	33.4

3.2. Mechanical Properties

In Table 3, mechanical properties were represented by the compressive and the flexural strength. The highest compressive strength was observed for the reference mortar (83.45 MPa) and decreased systematically with an increasing amount of CB to approximately 7.3 MPa (CB 2 and CB 2.25). The compressive strength of CB 1.5 was about 55% that of the reference mortar, whereas CB 2 and CB 2.25 were about 9%. The highest flexural strength was observed for the reference mortar (8.26 MPa) and decreased systematically with an increasing amount of CB to 2.4 MPa (CB 2.25), which was about 30% of the value for the reference mortar.

Table 3. Mechanical properties of the studied geopolymers.

	Compressive Strength (MPa)	Flexural Strength (MPa)
CB 0	83.45	8.26
CB 0.75	68.60	5.23
CB 1.25	46.49	5.21
CB 1.5	20.38	5.04
CB 1.75	17.00	3.75
CB 2	7.31	3.85
CB 2.25	7.31	2.40

3.3. Thermal and Electrical Properties

In Table 4, thermal properties were represented by the thermal conductivity, and the specific heat capacity and electrical properties were represented by the electrical conductivity. The highest thermal conductivity was observed for CB 0 ($\lambda = 1.71 \text{ W}\cdot\text{m}^{-1}\cdot\text{K}^{-1}$). The decreasing tendency of the thermal conductivity with an increasing amount of CB admixture corresponds with the basic physical properties (the bulk density was directly proportional, and the total open porosity was inversely proportional). CB 2.25 exhibited the lowest thermal conductivity ($0.63 \text{ W}\cdot\text{m}^{-1}\cdot\text{K}^{-1}$). The specific heat capacity of the mortars was in the range of $715\text{--}849 \text{ J}\cdot\text{kg}^{-1}\cdot\text{K}^{-1}$. The maximum value ($849 \text{ J}\cdot\text{kg}^{-1}\cdot\text{K}^{-1}$) was observed for CB 2.25. Higher values around $800 \text{ J}\cdot\text{kg}^{-1}\cdot\text{K}^{-1}$ were observed for the reference mortar CB 0 and the mortars with higher dosages of CB (CB 1.75, CB 2), whereas lower values ($715\text{--}733 \text{ J}\cdot\text{kg}^{-1}\cdot\text{K}^{-1}$) were observed for mortars with lower dosages of CB (CB 0.75, CB 1.25, CB 1.5).

Table 4. Thermal and electrical properties of the studied geopolymers.

	Thermal Conductivity ($\text{W}\cdot\text{m}^{-1}\cdot\text{K}^{-1}$)	Specific Heat Capacity ($\text{J}\cdot\text{kg}^{-1}\cdot\text{K}^{-1}$)	Electrical Conductivity ($\text{S}\cdot\text{m}^{-1}$)
CB 0	1.71	790	8.0×10^{-7}
CB 0.75	0.94	715	2.7×10^{-5}
CB 1.25	0.85	733	8.6×10^{-5}
CB 1.5	0.81	728	3.2×10^{-3}
CB 1.75	0.75	803	1.1×10^{-2}
CB 2	0.71	792	2.2×10^{-2}
CB 2.25	0.63	849	1.3×10^{-1}

The electrical conductivity increased significantly with an increasing amount of CB because of the formations of conductive paths within the geopolymer matrix. Such an increase is a very important assumption for self-heating ability of the tested mortars. The initial value of the electrically non-conductive mortar CB 0 ($8 \times 10^{-7} \Omega\cdot\text{m}$) improved to the highest value ($1.3 \times 10^{-1} \Omega\cdot\text{m}$) observed for CB 2.25, which was an increase of about 7 orders of magnitude. With respect to the measured data, it was expected that the percolation threshold for the self-heating ability would be at 1.5 wt. % of CB. The electrical conductivity of CB 1.5 mortar was 4000 times higher than that of the reference mortar ($3.2 \times 10^{-3} \Omega\cdot\text{m}$).

3.4. Self-Heating Ability

In Figures 3–14, self-heating experiments are presented. Each self-heating experiment involved the determination of time dependencies of the ambient temperature, the temperature of the sample, and the power (dependent on power supply voltage and the passing current). Self-heating experiments conducted at 40 V on CB 0, CB 0.75, and CB 1.25 (Figures 3–5) and at 100 V on CB 1.25 (Figure 6) confirmed the expectations obtained by measurements of electrical properties that such materials did not exhibit a self-heating ability. The passing current, which is directly proportional to the measured

power P (W), was negligible or very low in evolving the Joule heat. Heating was not possible even after the voltage increased from 40 to 100 V.

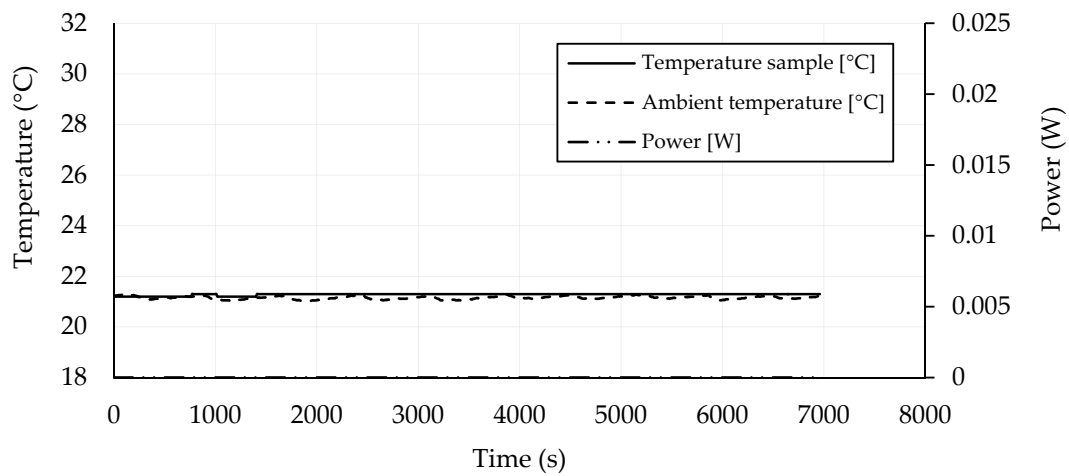


Figure 3. Self-heating experiment—CB 0, 40 V.

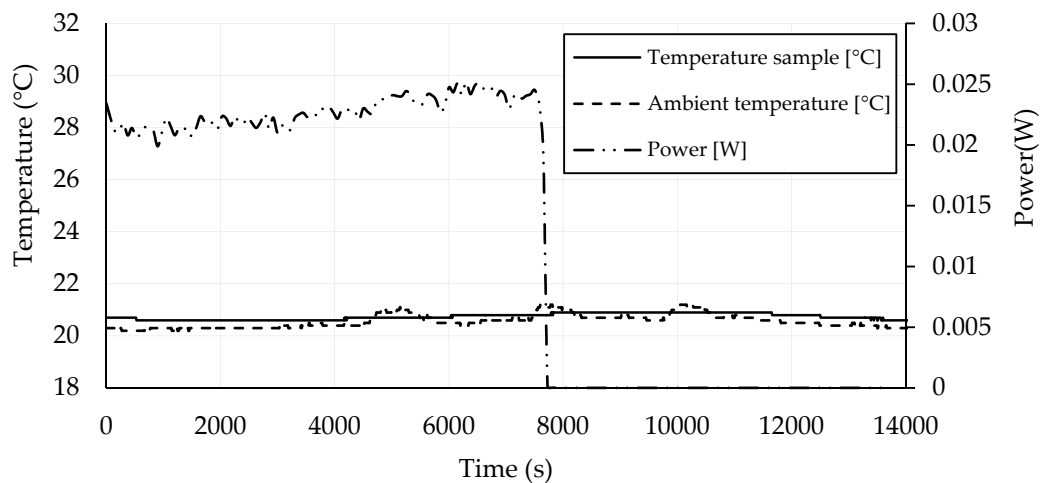


Figure 4. Self-heating experiment—CB 0.75, 40 V.

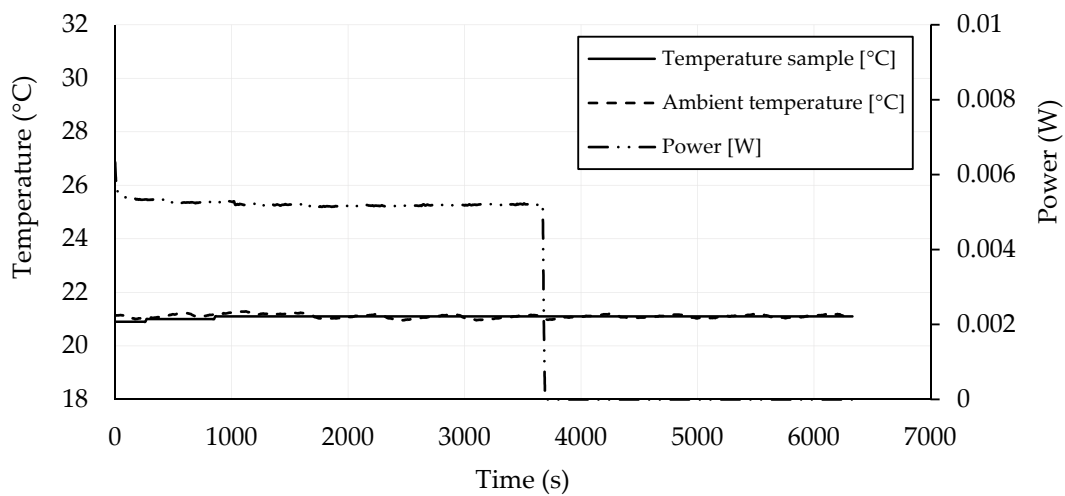


Figure 5. Self-heating experiment—CB 1.25, 40 V.

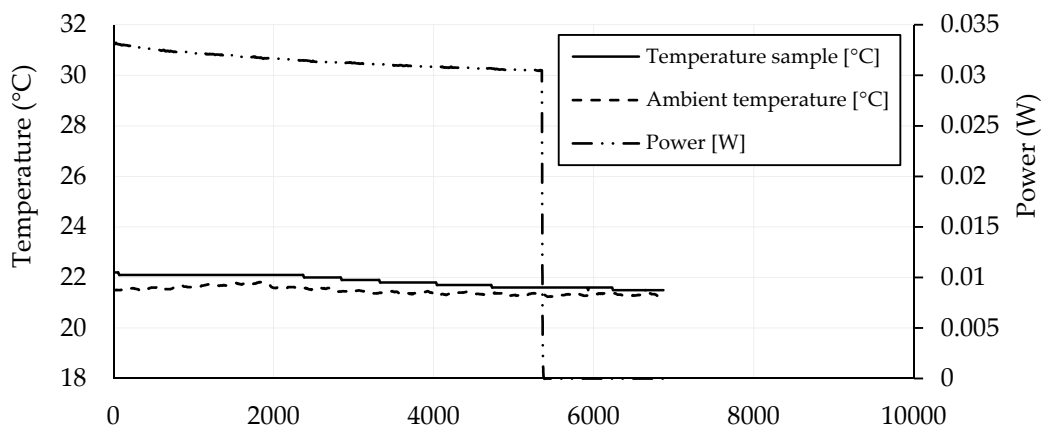


Figure 6. Self-heating experiment—CB 1.25, 100 V.

A low self-heating ability was observed for CB 1.5 at 40 V, where $\Delta t \approx 2\text{ }^\circ\text{C}$ and $P \approx 0.21\text{ W}$ (Figure 7). An increased passing current induced by an increase of the voltage level from 40 to 100 V resulted in a temperature increase of $\Delta t \approx 9.5\text{ }^\circ\text{C}$ with the corresponding power $P \approx 1.18\text{ W}$ (Figure 8).

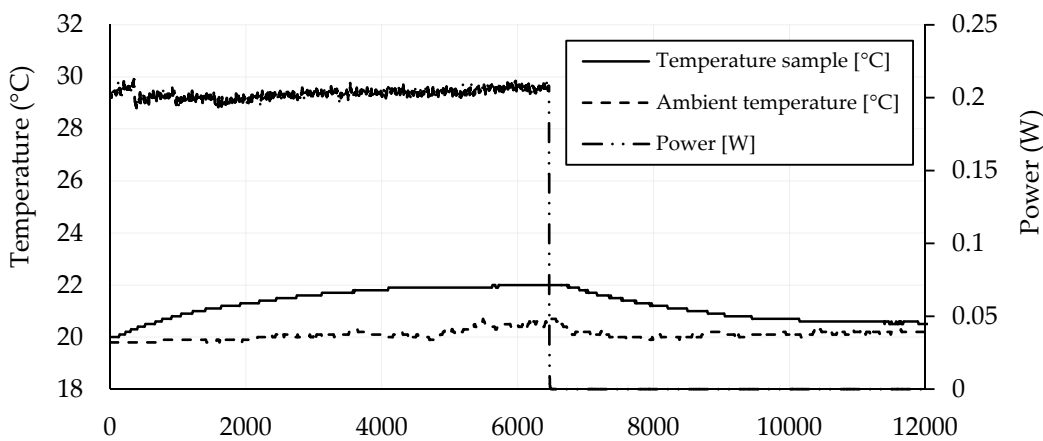


Figure 7. Self-heating experiment—CB 1.5, 40 V.

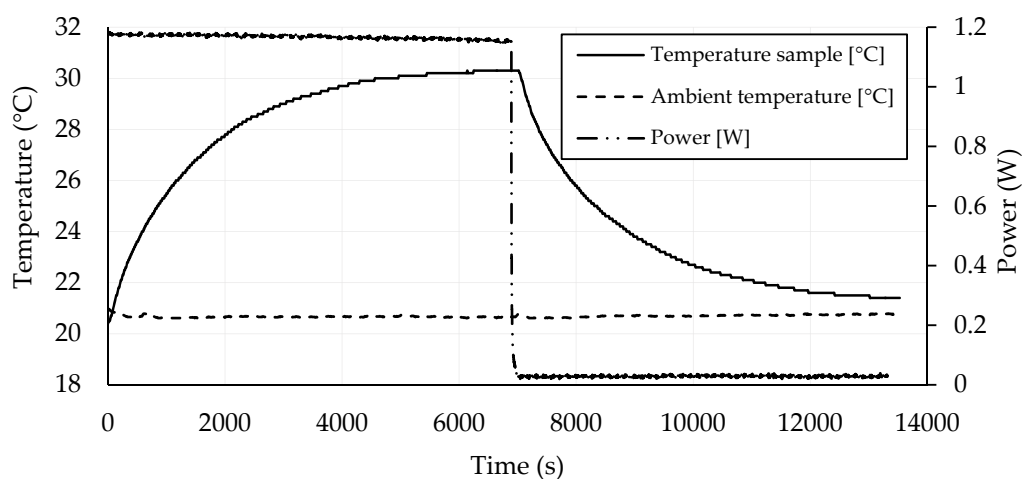


Figure 8. Self-heating experiment—CB 1.5, 100 V.

CB 1.75 exhibited a slightly better self-heating performance than the geopolymer mortars with a lower amount of CB. At 40 V, $\Delta t \approx 3\text{ }^\circ\text{C}$ and $P \approx 0.51\text{ W}$ were achieved (Figure 9). At 100 V, further increases in the temperature $\Delta t \approx 22\text{ }^\circ\text{C}$ and the power $P \approx 3.45\text{ W}$ were observed (Figure 10). CB 2

exhibited a good self-heating performance at 40 V, where $\Delta t \approx 10\text{ }^\circ\text{C}$ and $P \approx 1.25\text{ W}$ (Figure 11), and at 100 V, where $\Delta t \approx 50\text{ }^\circ\text{C}$ and $P \approx 7.41\text{ W}$ were achieved (Figure 12).

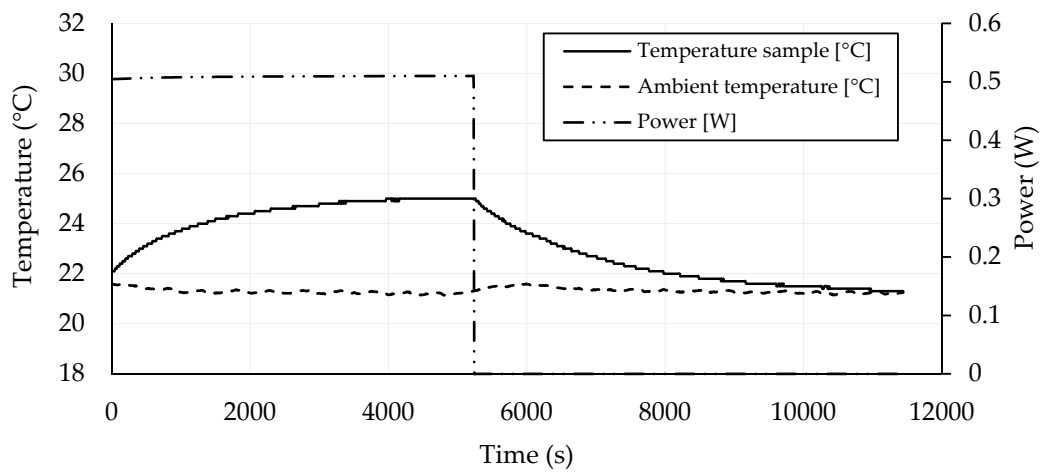


Figure 9. Self-heating experiment—CB 1.75, 40 V.

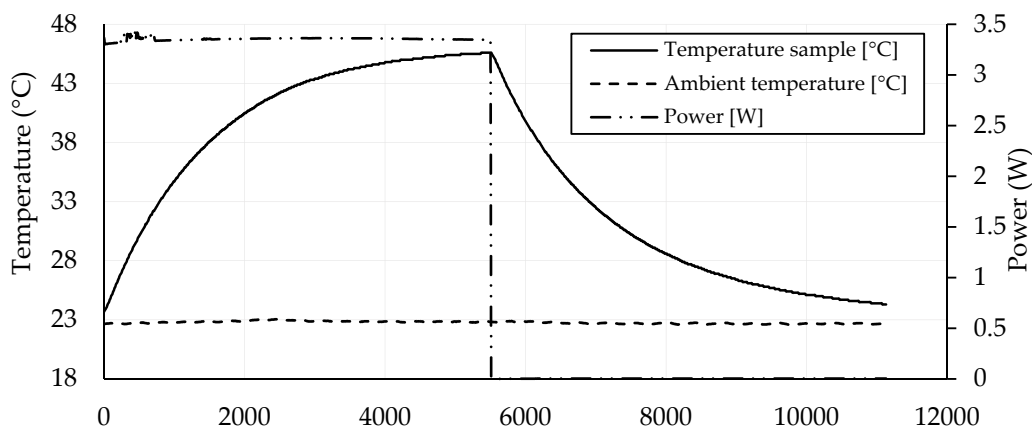


Figure 10. Self-heating experiment—CB 1.75, 100 V.

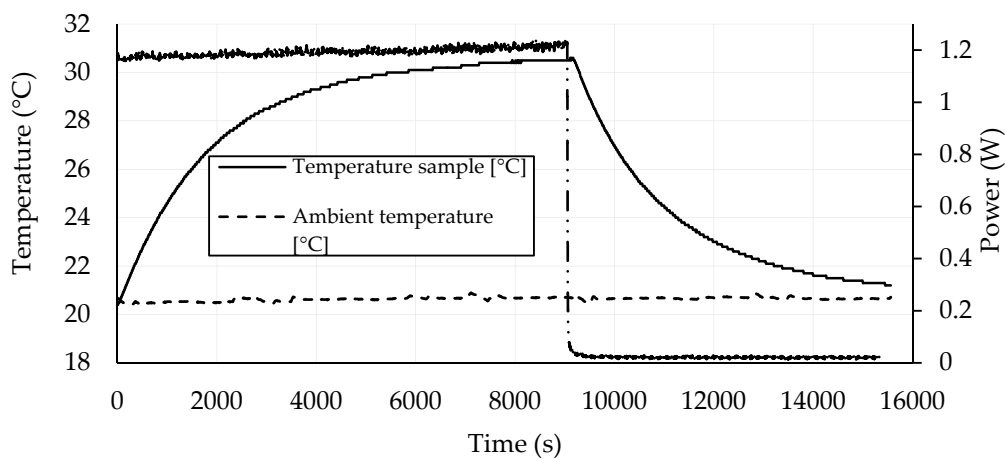


Figure 11. Self-heating experiment—CB 2, 40 V.

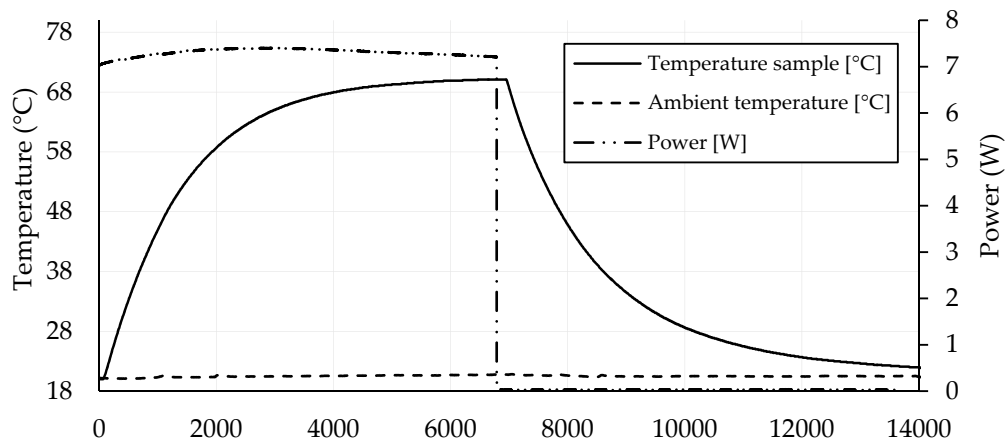


Figure 12. Self-heating experiment—CB 2, 100 V.

CB 2.25 exhibited the best self-heating performance. At 40 V, $\Delta t \approx 26$ °C and $P \approx 3.63$ W were achieved (Figure 13), and at 100 V the temperature increase was $\Delta t \approx 110$ °C and the corresponding power P was 25.99 W (Figure 14).

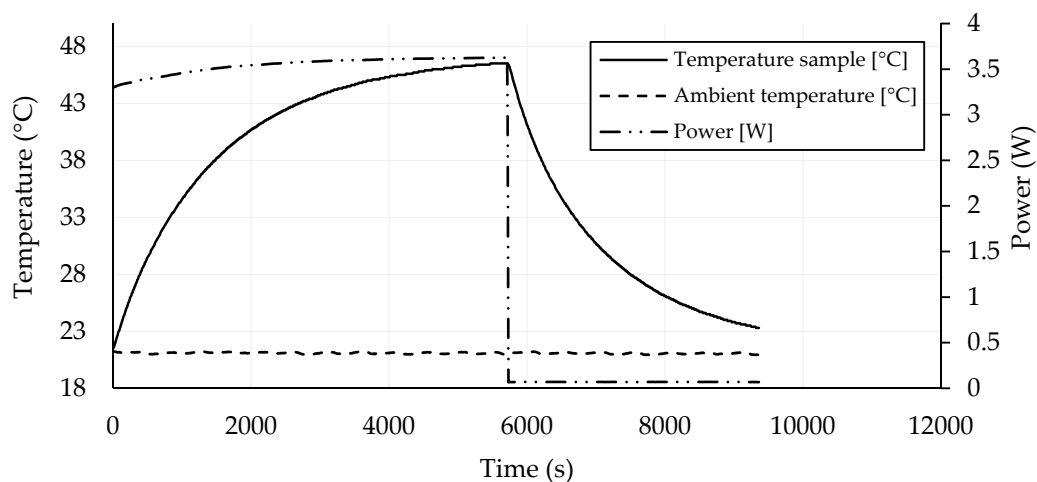


Figure 13. Self-heating experiment—CB 2.25, 40 V.

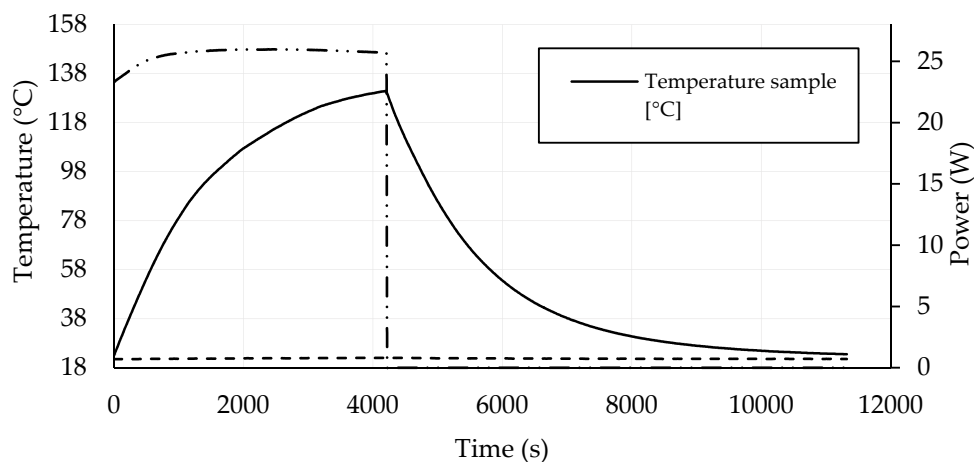


Figure 14. Self-heating experiment—CB 2.25, 100 V.

In Figure 15a, the maximal values of power from the conducted self-heating experiments loaded by 40 and 100 V are summarized. Geopolymer mortars with an amount of CB admixture starting

at 1.5 wt. % were able to generate heat, leading to a temperature increase at both voltage levels. Comparing the heating power at 40 and 100 V of the mortars able to evolve heat, the highest increase was achieved for CB 2.25 (7.2 times higher power at 100 V than at 40 V), whereas the lowest non-zero increase was for CB 1.5 (5.6 times higher power at 100 V than at 40 V). In Figure 15b, the maximal achieved temperatures of the mortars during the self-heating experiments and the compressive strengths are presented. Quantities exhibited the opposite trend, where higher temperatures were achieved with an increasing amount of CB, but mechanical properties deteriorated.

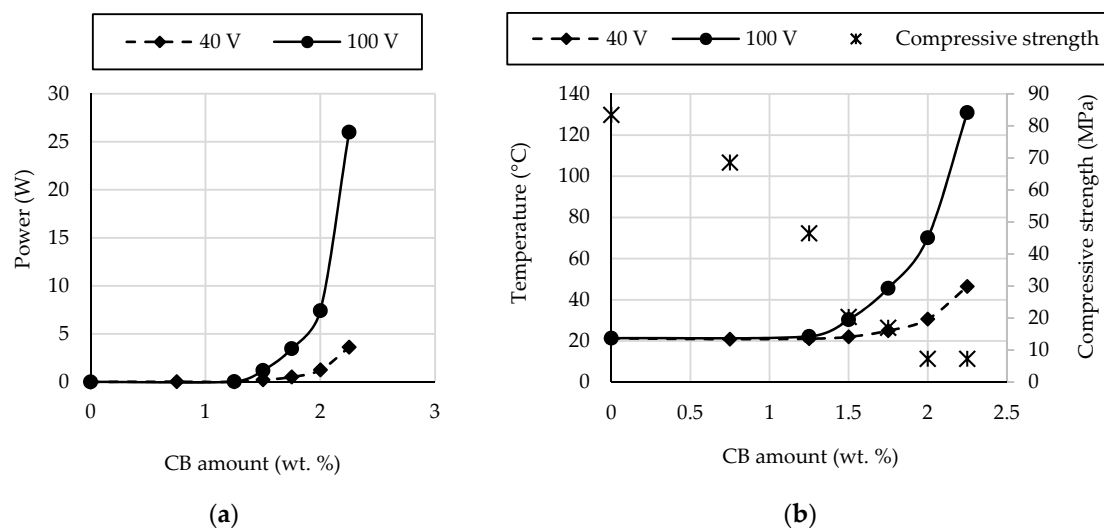


Figure 15. Dependence of (a) the power on CB amount (40 V, 100 V); (b) maximal achieved temperature and the compressive strength on CB amount (40 V, 100 V).

4. Discussion

With respect to the data presented in Tables 2 and 3, decreases in the bulk density, compressive strength, and flexural strength and an increase in the total open porosity of the designed geopolymers were observed with an increasing amount of CB admixture. This mainly was due to the high surface area of particles and aggregated clusters of particles of such ECA filler (Figure 1). The average grain size of CB was $d_{50} = 0.52 \mu\text{m}$ and $d_{90} = 17.6 \mu\text{m}$, which was significantly lower compared to the grain size of the slag binder ($d_{50} = 15.5 \mu\text{m}$ and $d_{90} = 38.3 \mu\text{m}$). Because of the high surface area of CB, more mixing water was needed (Table 1), which resulted in an increase in the total open porosity. However, an increased amount of water was necessary for the preparation of mixtures with plastic consistencies with an average base diameter equal to 160 mm according to the ČSN EN 1015-3 standard Determination of Consistency of Fresh Mortar by Flow Table. The highest decrease in bulk density and the highest increase in total open porosity observed between the reference mortar (CB 0) and the mortar with the highest amount of CB (CB 2.25) were about 18.5% and 90%.

Mechanical properties of the mortars with higher CB dosages were negatively influenced by an increased total open porosity. The compressive strength of CB 0 (83.45 MPa) was significantly higher compared to that of the mortars with the self-heating ability. The decrease was significant (CB 1.5 about 76% compared to CB 0), but remained at a good level (20.38 MPa up to 1.5 wt. % of CB admixture). Geopolymer mortars with an amount of CB higher than 1.75 wt. % exhibited low compressive strength, equal to 7.31 MPa, which was about a 91% decrease compared to the reference mortar. However, it should be noted that the compressive strength of cementitious mortars widely used in practice with aggregates up to 2 mm is usually up to 10 MPa. In the case of the flexural strength, the highest value was observed for CB 0 (8.26 MPa) and decreased with an increasing amount of CB, but not as much as in the case of the compressive strength (CB 2.25 compared to CB 0, about a 71% decrease). Taking into consideration cement mortars widely used in practice with flexural strengths up to 2.5 MPa, all the designed geopolymer mortars are comparable.

The thermal conductivity, an important parameter describing the ability of effective spreading of the generated Joule heat, exhibited a decreasing tendency with an increasing amount of CB, which was influenced, again, by the increasing porosity. The highest thermal conductivity was observed for CB 0 ($1.71 \text{ W}\cdot\text{m}^{-1}\cdot\text{K}^{-1}$), whereas the lowest was observed for CB 2.25 ($0.63 \text{ W}\cdot\text{m}^{-1}\cdot\text{K}^{-1}$). The thermal conductivity of all the mortars with CB admixtures was below $1 \text{ W}\cdot\text{m}^{-1}\cdot\text{K}^{-1}$. The specific heat capacity of the mortars ranged between $715\text{--}849 \text{ J}\cdot\text{kg}^{-1}\cdot\text{K}^{-1}$. Higher values around $800 \text{ J}\cdot\text{kg}^{-1}\cdot\text{K}^{-1}$ were observed for the reference mortar CB 0 and the mortars with higher dosages of CB (CB 1.75, CB 2), whereas lower values ($715\text{--}733 \text{ J}\cdot\text{kg}^{-1}\cdot\text{K}^{-1}$) were observed for mortars with lower dosages of CB (CB 0.75, CB 1.25, CB 1.5). The maximum value ($849 \text{ J}\cdot\text{kg}^{-1}\cdot\text{K}^{-1}$) was observed for CB 2.25.

Electrical properties represented by the electrical conductivity were essential in terms of the main aim of this paper, which was the design of multifunctional geopolymers. The self-heating ability can be achieved just by significantly increasing the electrical conductivity. The reference mortar was a typical electrical insulator with an electrical conductivity of $8.0 \times 10^{-7} \text{ S}\cdot\text{m}^{-1}$; therefore, it was not able to generate Joule heat. The electrical conductivity increased by 1 order of magnitude for CB 0.75 and 2 orders of magnitude for CB 1.25, which was not sufficient. The electrical conductivity of CB 1.5 increased by about 3 orders of magnitude, which was close to the percolation threshold, and the slight self-heating ability of this mortar was further observed. Further improvement was observed for CB 1.75 (4 orders of magnitude), CB 2 (4 orders of magnitude), and CB 2.25 (5 orders of magnitude), which demonstrated a significant enhancement of electrical properties.

Self-heating experiments proved a slight self-heating ability of CB 1.5 at 40 V, and a power 0.21 W was able to heat up the sample by about 2°C . At 40 V loading, the power increased with increasing the amount of CB in the following way: CB 1.75, 0.51 W; CB 2, 1.25 W; and CB 2.25, 3.63 W; with corresponding temperature increases of CB 1.75, 3°C ; CB 2, 10°C ; and CB 2.25, 26°C . At 100 V loading, the powers of CB 1.5, CB 1.75, CB 2, and CB 2.25 were 1.18, 3.45, 7.41, and 25.99 W, and temperature increases were 9.5, 22, 50, and 110°C , respectively. It is evident that an increase in the applied voltage from 40 to 100 V leads to a significantly higher self-heating ability. In Figure 15b, the maximal achieved temperatures are presented together with the compressive strength dependent on the amount of CB. Despite the fact that the mechanical properties of geopolymer mortars with the CB admixture are significantly lower compared to the reference mortar, their mechanical properties are comparable to, or even better than, commonly used cementitious mortars, and such types of material can find applications in the construction industry.

5. Conclusions

A conducted investigation on the basic physical, mechanical, thermal, electrical properties, and the self-heating ability of alkali-activated slag mortars with carbon black as a conductive filler is presented in this paper, and the following conclusions have been drawn from the experimental results:

- An increase in the amount of CB admixture in geopolymers based on GBFS activated by water glass led to the deterioration of mechanical properties, which was attributed to an increased amount of mixing water and, consequently, increased porosity.
- An increase in the amount of CB admixture in geopolymers based on GBFS activated by water glass led to a decrease in thermal conductivity, which is an important parameter describing the ability to spread the evolved heat.
- The percolation threshold for the self-heating ability was around 1.5 wt. % of CB, where a slight self-heating ability was observed.
- Geopolymers based on GBFS activated by water glass with CB amounts in the range of 1.75–2.25 wt. % exhibited good self-heating abilities.
- The self-heating ability of geopolymers based on GBFS activated by water glass with CB can be significantly improved by increasing the voltage. The heating power of the geopolymer mortar

with CB in the amount of 2.25 wt. % at 40 V was similar to the heating power of the geopolymers mortar with CB in the amount of 1.75 wt. % at 100 V (3.63 vs. 3.45 W).

This study proved the possibility to design multifunctional geopolymers with self-heating abilities based on alkali-activated GBFS and CB admixture. However, further investigation is necessary, especially in terms of optimizing the designed mixtures leading to a decrease in the porosity and in an effective homogenization of CB, which will ensure maximization of the self-heating ability with a lower deterioration of mechanical properties.

Author Contributions: Writing—original draft, Methodology, Resources, L.F.; Experimental—electrical properties, thermal properties, self-heating experiment, M.P.; Methodology, Resources, W.-T.L.; Experimental—basic physical properties, mechanical properties, L.P.; Supervision, R.Č.

Funding: This research was funded by the Czech Science Foundation under the project No. 19-11516S, Ministry of Science and Technology (MOST, Taiwan) under the project MOST-108-2221-E-197-006, and Ministry of Industry and Trade of the Czech Republic under innovation voucher No. CZ.011.02/0.0/17_115/0012287.

Conflicts of Interest: The authors declare no conflicts of interest.

References

1. Han, B.G.; Wang, Y.Y.; Dong, S.F.; Zhang, L.Q.; Ding, S.Q.; Yu, X.; Ou, J.P. Smart concretes and structures: A review. *J. Intell. Mater. Syst. Struct.* **2015**, *26*, 1303–1345. [[CrossRef](#)]
2. Rana, S.; Subramani, P.; Figueiro, R.; Correia, A.G. A review on smart self-sensing composite materials for civil engineering applications. *Aims Mater. Sci.* **2016**, *3*, 357–379. [[CrossRef](#)]
3. Han, B.; Sun, S.; Ding, S.; Zhang, L.; Yu, X.; Ou, J. Review of nanocarbon-engineered multifunctional cementitious composites. *Compos. Part A Appl. Sci. Manuf.* **2015**, *70*, 69–81. [[CrossRef](#)]
4. Li, Z.; Ding, S.; Yu, X.; Han, B.; Ou, J. Multifunctional cementitious composites modified with nano titanium dioxide: A review. *Compos. Part A: Appl. Sci. Manuf.* **2018**, *111*, 115–137. [[CrossRef](#)]
5. Pisello, A.L.; D'Alessandro, A.; Sambuco, S.; Rallini, M.; Ubertini, F.; Asdrubali, F.; Materazzi, A.L.; Cotana, F. Multipurpose experimental characterization of smart nanocomposite cement-based materials for thermal-energy efficiency and strain-sensing capability. *Sol. Energy Mater. Sol. Cells* **2017**, *161*, 77–88. [[CrossRef](#)]
6. Chung, D.D.L. Self-heating structural materials. *Smart Mater. Struct.* **2004**, *13*, 562–565. [[CrossRef](#)]
7. Gomis, J.; Galao, O.; Gomis, V.; Zornoza, E.; Garces, P. Self-heating and deicing conductive cement. Experimental study and modeling. *Constr. Build. Mater.* **2015**, *75*, 442–449. [[CrossRef](#)]
8. Armoosh, S.R.; Oltulu, M. Self-heating of electrically conductive metal-cementitious composites. *J. Intell. Mater. Syst. Struct.* **2019**, *30*, 2234–2240. [[CrossRef](#)]
9. Armoosh, S.R.; Oltulu, M. Effect of Different Micro Metal Powders on the Electrical Resistivity of Cementitious Composites. In Proceedings of the 3rd World Multidisciplinary Civil Engineering, Architecture, Urban Planning Symposium, Prague, Czech Republic, 18–22 June 2018; Volume 471.
10. Wei, J.; Zhao, L.; Zhang, Q.; Nie, Z.; Hao, L. Enhanced thermoelectric properties of cement-based composites with expanded graphite for climate adaptation and large-scale energy harvesting. *Energy Build.* **2018**, *159*, 66–74. [[CrossRef](#)]
11. Wei, J.; Fan, Y.; Zhao, L.; Xue, F.; Hao, L.; Zhang, Q. Thermoelectric properties of carbon nanotube reinforced cement-based composites fabricated by compression shear. *Ceram. Int.* **2018**, *44*, 5829–5833. [[CrossRef](#)]
12. Wei, J.; Nie, Z.; He, G.; Hao, L.; Zhao, L.; Zhang, Q. Energy harvesting from solar irradiation in cities using the thermoelectric behavior of carbon fiber reinforced cement composites. *RSC Adv.* **2014**, *4*, 48128–48134. [[CrossRef](#)]
13. Ali, M.; Saidur, R.; Hossain, M. A review on emission analysis in cement industries. *Renew. Sustain. Energy Rev.* **2011**, *15*, 2252–2261. [[CrossRef](#)]
14. Wei, J.X.; Cen, K.; Geng, Y.B. Evaluation and mitigation of cement CO₂ emissions: Projection of emission scenarios toward 2030 in China and proposal of the roadmap to a low-carbon world by 2050. *Mitig. Adapt. Strateg. Glob. Chang.* **2019**, *24*, 301–328. [[CrossRef](#)]
15. Andrew, R.M. Global CO₂ emissions from cement production, 1928–2017. *Earth Syst. Sci. Data* **2018**, *10*, 2213–2239. [[CrossRef](#)]

16. Mehta, A.; Siddique, R. An overview of geopolymers derived from industrial by-products. *Constr. Build. Mater.* **2016**, *127*, 183–198. [[CrossRef](#)]
17. Ma, C.-K.; Awang, A.Z.; Omar, W. Structural and material performance of geopolymer concrete: A review. *Constr. Build. Mater.* **2018**, *186*, 90–102. [[CrossRef](#)]
18. Albitar, M.; Ali, M.M.; Visintin, P.; Drechsler, M. Durability evaluation of geopolymer and conventional concretes. *Constr. Build. Mater.* **2017**, *136*, 374–385. [[CrossRef](#)]
19. Zuda, L.; Drchalova, J.; Rovnanik, P.; Bayer, P.; Keršner, Z.; Cerny, R. Alkali-activated aluminosilicate composite with heat-resistant lightweight aggregates exposed to high temperatures: Mechanical and water transport properties. *Cem. Concr. Compos.* **2010**, *32*, 157–163. [[CrossRef](#)]
20. Nguyen, T.H.Y.; Tsuchiya, K.; Atarashi, D. Microstructure and composition of fly ash and ground granulated blast furnace slag cement pastes in 42-month cured samples. *Constr. Build. Mater.* **2018**, *191*, 114–124. [[CrossRef](#)]
21. Davidovits, J. Geopolymers: Ceramic-Like Inorganic Polymers. *J. Ceram. Sci. Technol.* **2017**, *8*, 335–350.
22. Pacheco-Torgal, F.; Castro-Gomes, J.; Jalali, S. Alkali-activated binders: A review Part 1. Historical background, terminology, reaction mechanisms and hydration products. *Constr. Build. Mater.* **2008**, *22*, 1305–1314. [[CrossRef](#)]
23. Altan, E.; Erdoğan, S.T. Alkali activation of a slag at ambient and elevated temperatures. *Cem. Concr. Compos.* **2012**, *34*, 131–139. [[CrossRef](#)]
24. Ben Haha, M.; Le Saoût, G.; Winnefeld, F.; Lothenbach, B. Influence of activator type on hydration kinetics, hydrate assemblage and microstructural development of alkali activated blast-furnace slags. *Cem. Concr. Res.* **2011**, *41*, 301–310. [[CrossRef](#)]
25. Pacheco-Torgal, F.; Castro-Gomes, J.; Jalali, S. Alkali-activated binders: A review Part 2. About materials and binders manufacture. *Constr. Build. Mater.* **2018**, *22*, 1315–1322. [[CrossRef](#)]
26. Tang, Z.; Li, W.; Hu, Y.; Zhou, J.L.; Tam, V.W. Review on designs and properties of multifunctional alkali-activated materials (AAMs). *Constr. Build. Mater.* **2019**, *200*, 474–489. [[CrossRef](#)]
27. Rovnanik, P.; Kusák, I.; Bayer, P.; Schmid, P.; Fiala, L. Comparison of electrical and self-sensing properties of Portland cement and alkali-activated slag mortars. *Cem. Concr. Res.* **2019**, *118*, 84–91. [[CrossRef](#)]
28. Rovnanik, P.; Kusak, I.; Bayer, P.; Schmid, P.; Fiala, L. Electrical and Self-Sensing Properties of Alkali-Activated Slag Composite with Graphite Filler. *Materials* **2019**, *12*, 1616. [[CrossRef](#)]
29. Fiala, L.; Rovnanik, P.; Cerny, R. Investigation of the Joule's effect in electrically enhanced alkali-activated aluminosilicates. *Cem. Wapno Beton* **2017**, *22*, 201–210.
30. Dhoble, Y.N.; Ahmed, S. Review on the innovative uses of steel slag for waste minimization. *J. Mater. Cycles Waste Manag.* **2018**, *20*, 1373–1382. [[CrossRef](#)]
31. Guo, J.; Bao, Y.; Wang, M. Steel slag in China: Treatment, recycling, and management. *Waste Manag.* **2018**, *78*, 318–330. [[CrossRef](#)]
32. Cabot Company. Cabot launches new carbon black products for tyre applications. *Addit. Polym.* **2014**, *2014*, 2. [[CrossRef](#)]
33. Li, Y.C.; Huang, X.R.; Zeng, L.J.; Li, R.F.; Tian, H.F.; Fu, X.W.; Wang, Y.; Zhong, W.H. A review of the electrical and mechanical properties of carbon nanofiller-reinforced polymer composites. *J. Mater. Sci.* **2019**, *54*, 1036–1076. [[CrossRef](#)]
34. Monteiro, A.O.; Cachim, P.B.; Costa, P.M. Self-sensing piezoresistive cement composite loaded with carbon black particles. *Cem. Concr. Compos.* **2017**, *81*, 59–65. [[CrossRef](#)]
35. Fiala, L.; Jerman, M.; Rovnaník, P.; Černý, R. Basic physical, mechanical and electrical properties of electrically enhanced alkali-activated aluminosilicates. *Mater. Tehnol.* **2017**, *51*, 1005–1009. [[CrossRef](#)]
36. Alonso, M.; Gismera, S.; Blanco, M.; Lanzón, M.; Puertas, F. Alkali-activated mortars: Workability and rheological behaviour. *Constr. Build. Mater.* **2017**, *145*, 576–587. [[CrossRef](#)]

